

The Mechanism of HIV-1 Core Assembly: Insights from Three-Dimensional Reconstructions of Authentic Virions

John A.G. Briggs,^{1,4} Kay Grünewald,² Bärbel Glass,³ Friedrich Förster,² Hans-Georg Kräusslich,³ and Stephen D. Fuller^{1,*}

¹Division of Structural Biology
Wellcome Trust Centre for Human Genetics
University of Oxford
Roosevelt Drive
Headington, Oxford, OX3 7BN
United Kingdom

²Department of Molecular Structural Biology
Max-Planck-Institut für Biochemie
D-82152 Martinsried
Germany

³Department of Virology
Universitätsklinikum Heidelberg
Im Neuenheimer Feld 324
D-69120 Heidelberg
Germany

Summary

Infectious HIV particles contain a characteristic cone-shaped core encasing the viral RNA and replication proteins. The core exhibits significant heterogeneity in size and shape, yet consistently forms a well-defined structure. The mechanism by which the core is assembled in the maturing virion remains poorly understood. Using cryo-electron tomography, we have produced three-dimensional reconstructions of authentic, unstained HIV-1. These reveal the viral morphology with unprecedented clarity and suggest the following mechanism for core formation inside the extracellular virion: core growth initiates at the narrow end of the cone and proceeds toward the distal side of the virion until limited by the viral membrane. Curvature and closure of the broad end of the core are then directed by the inner surface of the viral membrane. This mechanism accommodates significant flexibility in lattice growth while ensuring the closure of cores of variable size and shape.

Introduction

Human immunodeficiency virus (HIV) buds from the membrane of an infected cell in an immature, noninfectious form (Swanstrom and Wills, 1997). The viral particles are mostly spherical and have a variable diameter (Briggs et al., 2003; Fuller et al., 1997; Wilk et al., 2001). This heterogeneity is a general feature of retroviruses (Briggs et al., 2004b; Kingston et al., 2001; Yeager et al., 1998). In immature HIV particles, the major structural protein, Gag, is arranged in a radial fashion, with the N-terminal matrix (MA) domain associated with the

viral membrane, followed by the internal capsid (CA) domain and the C-terminal nucleocapsid (NC) domain pointed toward the center (Fuller et al., 1997; Wilk et al., 2001). During or shortly after budding, Gag is cleaved by the viral protease, leading to virus maturation, which is reflected in a dramatic morphological change required for infectivity (Swanstrom and Wills, 1997; Vogt, 1997). Maturation requires disassembly of the immature Gag shell, followed by a second assembly step leading to the mature core (Briggs et al., 2004a). The MA domains remain associated with the viral membrane, while the ribonucleoprotein (RNP) complex of NC and genomic RNA condenses in the center. The CA domains form the typical cone-shaped core of mature HIV encasing the RNP. Formation of the mature core requires only a fraction of the available CA molecules (Briggs et al., 2004a), and it may depend on nucleation by the viral genome (Briggs et al., 2003).

Important information regarding the structure of the HIV core has been derived from analysis of in vitro-assembled core-like particles. Purified CA and CA-NC proteins assemble, under certain conditions, into conical particles that closely resemble the authentic HIV core (Ganser et al., 1999). From these studies, Ganser et al. (1999) proposed that the HIV-1 core adopts the symmetry of a fullerene-type cone, forming a curved p6 lattice, with 12, unevenly distributed, pentameric defects. The placement of five of these defects at the narrow end of the cone, and seven at the broad end, allows for formation of a range of conical structures analogous to the cones formed by elemental carbon (Ge and Sattler, 1994). These cones exhibit a predicted mean included angle of 19.2° found in the lowest angle fullerene cones (Ge and Sattler, 1994). The morphologies of cores observed in other retroviruses can be generated by altering the distribution of pentameric defects (Ganser-Pornillos et al., 2004). Cryo-electron microscopy has confirmed the presence of a p6 lattice in the in vitro-assembled particles (Li et al., 2000) and in authentic, mature HIV cores (Briggs et al., 2003). Furthermore, the mean included angle of conical cores conforms to the predicted value, as measured by electron microscopy (Briggs et al., 2003; Welker et al., 2000), and recently by cryo-electron tomography (cET), of HIV-derived virus-like particles (Benjamin et al., 2005).

The distinctive conical core of the mature HIV virion poses two intriguing questions. First, how do the properties of CA, and of the environment within the virus particle, determine the conical shape? Second, how do these properties produce cores that exhibit significant heterogeneity in both size and shape, but consistently form well-defined, complete structures? To address these questions, we have used cET of authentic HIV-1 particles to examine the three-dimensional (3D) structures of the viral cores. This method permits the 3D visualization of heterogeneous, asymmetrical macromolecular complexes at close to physiological conditions in vitreous buffer in the absence of stain (Baumeister et al., 1999; Grünewald et al., 2003). The method has important advantages for this study, since it preserves the

*Correspondence: stephen.fuller@strubi.ox.ac.uk

⁴Present address: Department of Chemistry and Biochemistry, Ludwig-Maximilians-Universität, Butenandtstrasse 11, 81377 Munich, Germany.

viral core and membrane intact, allowing us to examine the relationship between the viral membrane and the core structure in three dimensions. This was not possible in early tomographic studies of HIV that used conventional preparation techniques (Hoglund et al., 1992). Using cET, we produced 3D reconstructions of mature, authentic HIV-1 that suggest a mechanism for maturation: core growth initiates at the narrow end of the cone and proceeds toward the distal side of the virion until limited by the viral membrane.

Results

Virion Morphology

Concentrated, high-titer ($\sim 10^9$ infectious units per ml) preparations of HIV-1 particles with minimal contamination of cellular vesicles were obtained as described previously (Welker et al., 2000). The quality of the preparation can be judged from Figure 1A. The virus was inactivated by treatment with 1% paraformaldehyde for 30 min on ice, and was then vitrified for cET. For each specimen, a series of projection images was collected at 2° tilt increments covering a minimum angular range of -68° to $+64^\circ$. The images were computationally combined to reconstruct a 3D density map. Reconstructions of 75 individual virions were obtained from 3 tomographic tilt series. These reconstructions reveal the 3D morphology of the virus with a clarity not previously seen (Figure 1 and Movie S1, see the Supplemental Data available with this article online; Macromolecular Structure Database entry EMD-1155).

Virions were approximately spherical (Figure 1), with diameters between 106 and 183 nm. The mean diameter, 125 ± 14 nm, was slightly smaller than that observed previously (Briggs et al., 2003; Wilk et al., 2001), reflecting a variability between different retroviral preparations (Briggs et al., 2004b). Projecting densities are visible on the viral membrane that are likely to represent both viral and cellular membrane proteins. There was no obvious uniformity in the morphology or distribution of these projections. The 3D morphology of the viral core could be observed inside the virions (Figures 1A and 1C). Of the 75 particles observed, 5 contained no well-defined core, 63 contained a single core, 3 contained 1 complete and 1 partial or indistinct core, and 4 contained 2 cores. As previously described, double-cored particles were larger than single-cored particles (158 ± 19 nm and 122 ± 11 nm, respectively) (Briggs et al., 2003). Here, we found fewer double-cored particles than previously, correlating with the smaller mean diameter of virions. Loose, disordered aggregates of density were detected in the space between the core and the membrane (Figures 1A, 1C, and 2A, white arrow). These aggregates probably represent excess CA not incorporated into cores (Briggs et al., 2004a), and they may correspond to the previously described “lateral bodies” (Gelderblom et al., 1987).

The majority of single-cored virions contained a core with conical morphology ($n = 40$, 63%) (Figures 2A–2F), similar to that predicted for fullerene cones (Ganser et al., 1999; Ge and Sattler, 1994). The remaining 23 individual cores had tubular, triangular (Figure 2G), or irregular (Figure 2H) morphologies. These morphologies are consistent with those described previously by electron

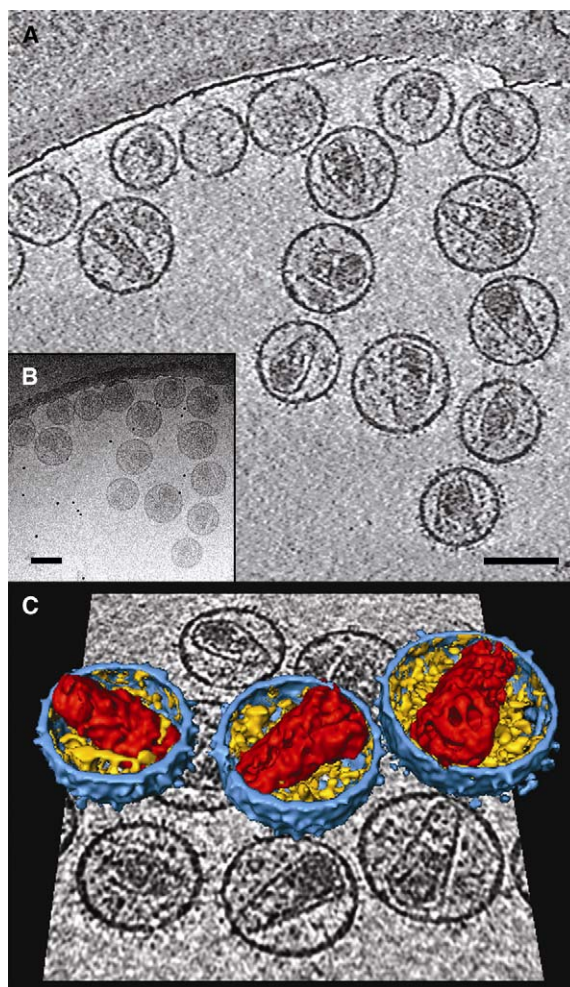


Figure 1. 3D Reconstruction of HIV-1 Virions from cET
(A) A central slice through one-quarter of the field of view in one of the cryo-electron tomograms. The scale bar is 100 nm.
(B) A single untilted image of the same area illustrating the even distribution of gold beads in the sample. The scale bar is 100 nm.
(C) 3D rendering of three sample virions from the tomogram. Blue, viral membrane; yellow, density between the membrane and the core; red, viral capsid. Half of the blue and yellow densities have been computationally removed to reveal the core. The rendered virions are shown above a central slice through the reconstruction. An animated version of this panel is available as Movie S1.

microscopy (Briggs et al., 2003; Welker et al., 2000) and recently by cET (Benjamin et al., 2005). Crosssections perpendicular to the axes of the conical cores were not circular, and, in some cases, they appeared faceted (data not shown). This observation is expected for fullerene cones, since the pentameric defects are not uniformly distributed. A region of high density was seen within the cores, likely representing the RNP complex of the viral genome with NC (Figure 2). This feature was not uniformly distributed or consistently positioned within the cores, but it was found predominantly at the broad end of cores, as previously observed (Briggs et al., 2003).

In some cores, a second layer of density was visible within the core, approximately parallel to the core edge. This layer could be observed at positions along the sides and broad ends of cores (Figures 2B and 2C,

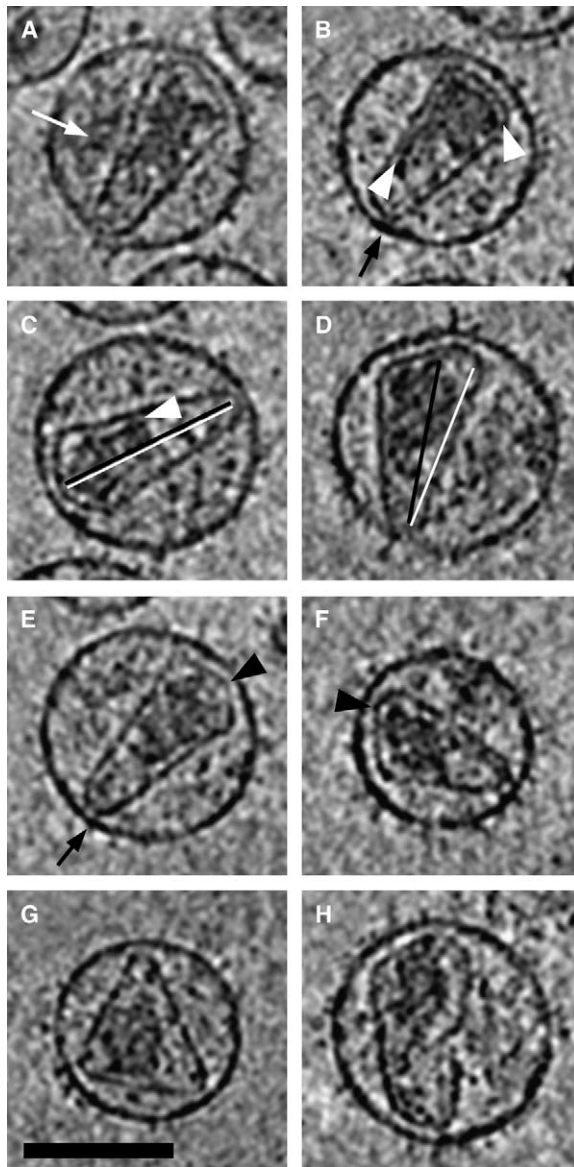


Figure 2. Central Slices through Tomographic Reconstructions of Eight Sample Virions, Illustrating the Range of Sizes and Core Morphologies

Images were Gaussian filtered, but they were not enhanced further by computational denoising.

(A–F) Conical cores. Annotations indicate examples of features referred to in the text. White arrow, putative lateral body; white arrowhead, double-layered region of core; white line, core’s longest axis; black line, core’s central axis; black arrow, density between the narrow end of the core and the membrane; black arrowhead, junction between facets at the broad end of the cone.

(G) Triangular core. The scale bar is 100 nm.

(H) Irregular core.

white arrowheads). It was found at a minimal distance of 8 nm from the core edge, although, in some positions, this separation increased. The 8 nm distance is similar to the spacing between CA and NC in the immature Gag lattice (Wilk et al., 2001). This spacing may represent the closest possible approach between the layers. The inner layer appeared to be continuous with the diffuse density of the RNP complex, and in no case did it

form a complete shell. We propose that this layer, which was also observed in a recent cET analysis of HIV-1 virus-like particles (Benjamin et al., 2005), represents a denser region of RNP within the core.

The Relationship between the Core and the Membrane

Examination of the 3D density revealed that the longest axis of the conical cores always spanned the diameter of the virion, despite large variation in virion diameter (Figures 2A–2F). The central axis of the cones, however, varied in orientation relative to the long axis (Figures 2C and 2D). This implies variability in the structural relationship between the broad end of the core and its edges. The broad end of the core appeared closed and followed the edge of the virion with an average spacing of approximately 12 nm (Figures 2A–2F). This spacing is similar to the distance between the membrane and the CA layer of Gag in immature HIV (Wilk et al., 2001). As observed in 2D images of isolated cores (Briggs et al., 2003; Welker et al., 2000), the broad end of the core appears not to be uniformly curved, but to have facets. It approaches closest to the membrane at the pointed junctions between these facets (Figures 2E and 2F, black arrowheads). The narrow ends of the cones, on the other hand, appeared to approach the membrane more closely than the broad ends (see Figures 2B–2E), and, in some cases, density was visible between the narrow end of the cone and the membrane (Figures 2B and 2E, black arrows). Previous studies have disagreed about the presence or absence of such a link (Benjamin et al., 2005; Briggs et al., 2003; Gelderblom, 1991; Hoglund et al., 1992). Description of the consistency of these features, and their composition or structure, will require further data collection, processing, and alignment.

The fact that most virions were approximately spherical in our preparation allowed us to explore the relationship between the dimensions of the core and the diameter of the virion. We measured the diameters of the caps at the broad and narrow ends, and the angle of the cone, for 24 cores with classical conical morphology (Figure 3). For each virion, these measurements were independently taken by three authors, and the average of the three measurements was used. We then determined correlations between the measured features and the virion diameter. The mean cone angle was $19.6^\circ \pm 2.1^\circ$ and did not vary systematically with virion diameter ($R^2 = 0.0005$). This angle is very close to the predicted value for a narrow-angled fullerene cone (19.2°), with five pentameric vertices at the narrow end. The cap at the narrow end of the cone had a diameter of 27 ± 2 nm, and it also did not vary systematically with virion diameter ($R^2 = 0.02$) (Figure 3). The diameter of the cap at the broad end of the core, on the other hand, was 56 ± 5 nm, and it showed a strong correlation with virion diameter ($R^2 = 0.75$) (Figure 3). Thus, the angle of the cone and the width at the narrow end of the cone are both independent of the dimensions of the virion, while the width at the broad end increases with increasing virion diameter.

Discussion

The observations reported in this study suggest a model for the mechanism of cone assembly. In this model,

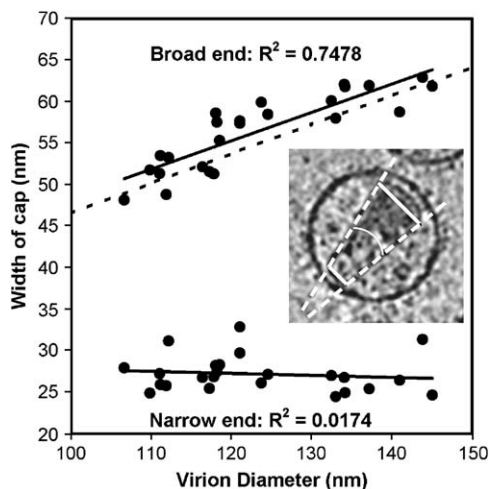


Figure 3. Relationship between the Widths of the Broad and Narrow Ends of Conical Cores and the Virion Diameter

Measurements were performed on individual 3D reconstructions by using Amira. Solid lines indicate the best linear fit to the data points. “R” is the linear correlation coefficient. The dashed line indicates the predicted relationship between the virion diameter and the broad end cap width, for the measured cone angle and narrow end cap width. The inset illustrates the measurements taken for a typical virion: the cone angle is the angle between the dashed, white lines; broad and narrow end core diameters were measured along the solid, white lines.

assembly of the mature cone, after disassembly of the Gag shell, initiates at the narrow end with an angle that is defined by fullerene geometry but is independent of virion size. Previous work suggests that, *in vivo*, core assembly requires a template in addition to the high CA concentration present inside the virion. This template may be the genome (Briggs et al., 2003), and/or a feature at the inside of the viral membrane, perhaps associated with the location where the virus membrane was severed from the cell during budding. Intriguingly, our reconstructions suggest a link between the narrow end of the core and the membrane in some particles. From the starting structure, the core would grow toward the distal side of the virion until further growth is constrained by the opposite edge of the virion. The length of the core would therefore, as observed, be dictated by the size of the virion, and the width of the broad end of the cone would, as observed, increase with increasing virion diameter (Figure 4). From the cone angle and the measured diameter of the narrow end of the core, it is possible to calculate the expected relationship between virion diameter and the diameter of the broad end of the cone. This predicted relationship (Figure 3, dotted line) is consistent with the measured diameters of the broad ends. The observed 12 nm spacing between the membrane and the broad end of the core is consistent with the spacing between the membrane and the CA layer being maintained either by specific or nonspecific steric interactions between the CA and the MA. These observations suggest that the curvature of the broad end is directed by growth along the inner surface of the membrane-*aposed* MA layer. By enforcing curvature, the membrane would promote the incorporation of pentameric defects, resulting in junctions between facets.

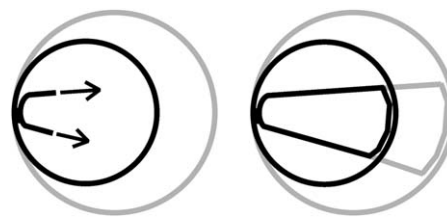


Figure 4. Proposed Model for Assembly of the Mature HIV Core

Core growth is illustrated in a small (black circle) and a large (gray circle) virion. Assembly initiates at the narrow end of the core, and a template such as the viral genome or a linkage to a feature of the viral envelope is used (left panel). The core grows with a preferential cone angle, defined by fullerene cone geometry, toward the distal side of the virion until contact with the distal membrane induces the introduction of additional pentameric positions and closure of the core (right panel). The larger virion therefore contains a larger core than the small virion.

The presence of triangular, tubular, and irregularly shaped cores in HIV preparations suggests that nucleation can also, at lower frequencies, lead to the creation of caps containing more or fewer than five pentameric vertices (Briggs et al., 2003; Ganser et al., 1999). Our observations of triangular (Figure 2G) and irregular (Figure 2H) cores are still consistent with the subsequent growth of these cores being limited by the viral membrane. Alternative models involving initiation of core assembly from the broad end (e.g., dictated by the relative amount of RNP present in the virion) cannot be formally excluded by our results, but are difficult to reconcile with the observed relationships between the broad ends of the core and the membrane.

In contrast to our results, HIV-derived virus-like particles were recently reported to show a consistent majority size and shape of the broad end of the core (Benjamin et al., 2005). In addition, these authors found the spacing between the narrow end of the core and the membrane to be the same as at the broad end, and they did not observe a core envelope linkage at the narrow end of the core (Benjamin et al., 2005). We believe that these discrepancies reflect differences in experimental methodology. The virions analyzed in our study were, to the best approximation, spherical (Figure 1), reducing the possibility that the spatial relationship between core and membrane is influenced by distortion of the membrane. In contrast, the virus-like particle preparation contained many nonspherical particles (Benjamin et al., 2005). Secondly, the limited angular range over which the sample can be imaged in cET causes a missing wedge (for single-axis tilt) or pyramid (for dual-axis tilt) of information in Fourier space, leading to smearing of the 3D reconstruction perpendicular to the ice layer. Since Benjamin et al. (2005) selected particles in which the core was oriented with its long axis perpendicular to the ice layer, this smearing will be most evident at the core ends and adjacent membrane in this case. Thirdly, we have used nearer to focus images (defocus of $-6 \mu\text{m}$ compared to $-16 \mu\text{m}$), which facilitate the visualization of finer details.

In vitro assembly of purified CA-NC protein can lead to assembly of cone-shaped cores (Ganser et al., 1999) that are capped at both ends. Hence, features other than the viral genome and/or budding scar can initiate

cone formation, and mechanisms other than the use of a constraining membrane can introduce broad end curvature. One possible mechanism would be an inherent tendency of the CA lattice toward curvature, due to, for example, a shorter optimal unit cell spacing in the C-terminal domain than in the N-terminal domain. As a cone grows toward its broad end, the radius of curvature of the lattice decreases, and a point may be reached at which it becomes more favorable to introduce pentameric defects, and maintain the radius of curvature, than to continue growth. In vivo, the radius of curvature is spatially limited by the RNP, which the core shell must encase, and by the viral membrane within which it must grow. This use of the membrane and the RNP to limit radius of curvature would permit retroviruses to accommodate significant heterogeneity and irregularity in the growing lattice, while still ensuring closure of the viral core.

The shapes and sizes of the viral cores are characteristically different in different retroviruses, raising the question of whether the described mechanism is universal among retroviruses. Examination of published cryo-electron micrographs of murine leukemia virus (Yeager et al., 1998), which exhibits an irregular polygonal mature core, shows that the core dimensions are very similar to the internal dimensions of the virion, and that the polygon vertices approach close to the viral membrane. This suggests that the membrane plays a role in promoting closure of the capsid shell in this virus as in HIV. In contrast, (although there are difficulties associated with interpreting projection images of asymmetric cores), cryo-electron micrographs of Rous sarcoma virus (Kingston et al., 2001) and mouse mammary tumor virus (Briggs et al., 2004b) do not consistently show the same close approach of the viral core to the membrane. This may suggest that the capsid proteins of these viruses preferentially assemble into a more tightly curved lattice, and pentameric vertices are therefore incorporated at a higher frequency. Immature HIV and Rous sarcoma virus particles do exhibit differences in preferred lattice curvature (Briggs et al., 2006).

In summary, our results suggest that assembly of the mature HIV-1 core initiates from the narrow end of the core, with core elongation being limited by the internal diameter of the virion. Growth then proceeds along the inner face of the envelope or the membrane-apposed MA layer to ensure closure of the broad end of cones of heterogeneous size and shape. This reconciles the apparent contradiction between the high heterogeneity of core sizes and shapes, and the consistency with which well-defined cores are formed. This mode of HIV core assembly would explain the formation of cores of variable sizes and shapes in virions of variable size.

Experimental Procedures

HIV-1 particles were prepared, purified, and inactivated as described (Welker et al., 2000). Samples were mixed with 10 nm colloidal gold and vitrified. cET was carried out by using a Phillips CM300FEG, equipped with a GATAN GIF 2002 postcolumn energy filter, and images were collected with a CCD camera. The microscope was operated at 300 kV and a magnification of 36,500 \times corresponding to a pixel size of 0.82 nm at the specimen level. A defocus level of $-6 \pm 0.5 \mu\text{m}$ was automatically maintained at the defocus spot during data collection (Koster et al., 1989). Thus, the

theoretical limit of resolution set by the contrast transfer function was 3.4 nm. Tilt series were collected automatically (Dierksen et al., 1992; Grimm et al., 1998), covering a minimum angular range from -68° to 64° at 2° increments with total doses not exceeding 50 electron/ \AA^2 . Alignment of projections with fiducial markers, and reconstructions, were performed by using the IMOD tomography processing package (Kremer et al., 1996). As images cannot be collected through the full 180° angular range, there is a missing wedge of information in the Fourier space representation of the density, leading the resolution of the reconstruction to be lower in the z direction than in the xy plane (Baumeister et al., 1999). Data were filtered to the first zero of the contrast transfer function prior to interpretation; however, the reconstruction contains no significant signal at resolutions better than 4 nm. The smallest spacing we have interpreted (the second layer of density within the core) is at 8 nm, which is coarser than would be predicted for first-order contrast transfer function artifacts at this defocus. Furthermore, the absence of a similar feature outside the core edge and the observed variation in the separation are not characteristic of contrast transfer function artifacts. Subtomograms containing individual virions were extracted by using the EM image processing package (Hegerl, 1996) and were analyzed before and after subjecting the tomograms to different levels of denoising by nonlinear anisotropic diffusion in edge enhancement mode (Frangakis and Hegerl, 2001). Visualization and segmentation was performed in Amira 3.1 (TGS, Bordeaux, France). Measurements of cone angles and dimensions were taken within planes containing the long axis of the cone, at a rotation around this axis minimizing the deleterious effects of the missing wedge of information.

Supplemental Data

Supplemental Data including an animated 3D reconstruction of HIV-1 virions are available at <http://www.structure.org/cgi/content/full/14/1/15/DC1/>.

Acknowledgments

J.A.G.B. was supported by a Wellcome Trust Structural Biology Studentship and is currently supported by a fellowship from the Alexander von Humboldt Foundation. S.D.F. is a Wellcome Trust Principal Research Fellow. The work was funded by the Wellcome Trust H5RCZRO (S.D.F., J.A.G.B.) and Deutsche Forschungsgemeinschaft grants GR1990/1-2 (K.G.) and SFB544, project B11 (H.-G.K.). We thank W. Baumeister for his support and encouragement, and B. Müller, B. Watson, and E. Majorovits for critical readings of the manuscript.

Received: July 5, 2005

Revised: September 1, 2005

Accepted: September 3, 2005

Published: January 10, 2006

References

- Baumeister, W., Grimm, R., and Walz, J. (1999). Electron tomography of molecules and cells. *Trends Cell Biol.* 9, 81–85.
- Benjamin, J., Ganser-Pornillos, B.K., Tivol, W.F., Sundquist, W.I., and Jensen, G.J. (2005). Three-dimensional structure of HIV-1 virus-like particles by electron cryotomography. *J. Mol. Biol.* 346, 577–588.
- Briggs, J.A.G., Wilk, T., Welker, R., Kräusslich, H.G., and Fuller, S.D. (2003). Structural organization of authentic, mature HIV-1 virions and cores. *EMBO J.* 22, 1707–1715.
- Briggs, J.A.G., Simon, M.N., Gross, I., Kräusslich, H.G., Fuller, S.D., Vogt, V.M., and Johnson, M.C. (2004a). The stoichiometry of Gag protein in HIV-1. *Nat. Struct. Mol. Biol.* 11, 672–675.
- Briggs, J.A.G., Watson, B.E., Gowen, B.E., and Fuller, S.D. (2004b). Cryoelectron microscopy of mouse mammary tumor virus. *J. Virol.* 78, 2606–2608.
- Briggs, J.A.G., Johnson, M.C., Simon, M.N., Fuller, S.D., and Vogt, V.M. (2006). Cryo-electron microscopy reveals conserved and divergent features of Gag packing in immature particles of Rous sarcoma virus and human immunodeficiency virus. *J. Mol. Biol.* 355, 157–168.

- Dierksen, K., Typke, D., Hegerl, R., Koster, A.J., and Baumeister, W. (1992). Towards automatic electron tomography. *Ultramicroscopy* 40, 71–87.
- Frangakis, A.S., and Hegerl, R. (2001). Noise reduction in electron tomographic reconstructions using nonlinear anisotropic diffusion. *J. Struct. Biol.* 135, 239–250.
- Fuller, S.D., Wilk, T., Gowen, B.E., Kräusslich, H.G., and Vogt, V.M. (1997). Cryo-electron microscopy reveals ordered domains in the immature HIV-1 particle. *Curr. Biol.* 7, 729–738.
- Ganser, B.K., Li, S., Klishko, V.Y., Finch, J.T., and Sundquist, W.I. (1999). Assembly and analysis of conical models for the HIV-1 core. *Science* 283, 80–83.
- Ganser-Pornillos, B.K., von Schwedler, U.K., Stray, K.M., Aiken, C., and Sundquist, W.I. (2004). Assembly properties of the human immunodeficiency virus type 1 CA protein. *J. Virol.* 78, 2545–2552.
- Ge, M., and Sattler, K. (1994). Observation of fullerene cones. *Chem. Phys. Lett.* 220, 192–196.
- Gelderblom, H.R. (1991). Assembly and morphology of HIV: potential effect of structure on viral function. *AIDS* 5, 617–638.
- Gelderblom, H.R., Hausmann, E.H.S., Örzal, M., Pauli, G., and Koch, M.A. (1987). Fine structure of human immunodeficiency virus (HIV) and immunolocalization of structural proteins. *Virology* 156, 171–176.
- Grimm, R., Singh, H., Rachel, R., Typke, D., Zillig, W., and Baumeister, W. (1998). Electron tomography of ice-embedded prokaryotic cells. *Biophys. J.* 74, 1031–1042.
- Grunewald, K., Desai, P., Winkler, D.C., Heymann, J.B., Belnap, D.M., Baumeister, W., and Steven, A.C. (2003). Three-dimensional structure of herpes simplex virus from cryo- electron tomography. *Science* 302, 1396–1398.
- Hegerl, R. (1996). The EM program package: a platform for image processing in biological electron microscopy. *J. Struct. Biol.* 116, 30–34.
- Hoglund, S., Ofverstedt, L.G., Nilsson, A., Lundquist, P., Gelderblom, H., Ozel, M., and Skoglund, U. (1992). Spatial visualization of the maturing HIV-1 core and its linkage to the envelope. *AIDS Res. Hum. Retroviruses* 8, 1–7.
- Kingston, R.L., Olson, N.H., and Vogt, V.M. (2001). The organization of mature Rous sarcoma virus as studied by cryoelectron microscopy. *J. Struct. Biol.* 136, 67–80.
- Koster, A.J., Deruijter, W.J., Vandenbos, A., and Vandermast, K.D. (1989). Autotuning of a TEM using minimum electron dose. *Ultramicroscopy* 27, 251–272.
- Kremer, J.R., Mastronarde, D.N., and McIntosh, J.R. (1996). Computer visualization of three-dimensional image data using IMOD. *J. Struct. Biol.* 116, 71–76.
- Li, S., Hill, C.P., Sundquist, W.I., and Finch, J.T. (2000). Image reconstructions of helical assemblies of the HIV-1 CA protein. *Nature* 407, 409–413.
- Swanstrom, R., and Wills, J.W. (1997). Synthesis, assembly, and processing of viral proteins. In *Retroviruses*, J.M. Coffin, S.H. Hughes, and H.E. Varmus, eds. (Cold Spring Harbor, New York: Cold Spring Harbor Laboratory Press), pp. 263–334.
- Vogt, V.M. (1997). Retroviral virions and genomes. In *Retroviruses*, J.M. Coffin, S.H. Hughes, and H.E. Varmus, eds. (Cold Spring Harbor, New York: Cold Spring Harbor Laboratory Press), pp. 27–69.
- Welker, R., Hohenberg, H., Tessmer, U., Huckhagel, C., and Kräusslich, H.G. (2000). Biochemical and structural analysis of isolated mature cores of human immunodeficiency virus type 1. *J. Virol.* 74, 1168–1177.
- Wilk, T., Gross, I., Gowen, B.E., Rutten, T., de Haas, F., Welker, R., Kräusslich, H.G., Boulanger, P., and Fuller, S.D. (2001). Organization of immature human immunodeficiency virus type 1. *J. Virol.* 75, 759–771.
- Yeager, M., Wilson-Kubalek, E.M., Weiner, S.G., Brown, P.O., and Rein, A. (1998). Supramolecular organization of immature and mature murine leukemia virus revealed by electron cryo-microscopy: implications for retroviral assembly mechanisms. *Proc. Natl. Acad. Sci. USA* 95, 7299–7304.

Accession Numbers

The tomographic map has been deposited in the Macromolecular Structure Database (<http://www.ebi.ac.uk/msd-srv/emdep/>) as entry EMD-1155.